ELSEVIER

Ceramics International 31 (2005) 1007–1013

CERAMICS INTERNATIONAL

www.elsevier.com/locate/ceramint

Wet forming and sintering behavior of nanometer-sized ceria powder

Yoshihiro Hirta*, Akito Harada, Xu Hong Wang

Department of Advanced Nanostructured Materials Science and Technology, Graduate School of Science and Engineering, Kagoshima University 1-21-40 Korimoto, Kagoshima 890-0065, Japan

Received 31 March 2004; received in revised form 23 October 2004; accepted 25 October 2004
Available online 13 January 2005

Abstract

An aqueous suspension of 25 vol.% ceria powder of 14 nm diameter (powder A) was consolidated by filtration through a gypsum mold. However, many cracks were formed during drying of the ceria compact. Addition of larger ceria powder of 37 nm diameter (powder B) to the 14 nm-ceria powder was effective to prevent the formation of cracks. The densification of the dried powder compacts with 90 vol.% powder A, 10 vol.% powder B was divided into four ranges with sintering temperature: range I (500–800 °C), sintering of primary particles within a secondary particle cluster; range II (800–1200 °C), grain growth of primary particles in a dense secondary particle cluster; range III (1200–1500 °C), sintering of dense secondary particle clusters with grain growth, and range IV (1500–1600 °C), grain growth of dense secondary particle clusters. Increased fraction of powder B to 40–60 vol.% suppressed the decrease of specific surface area of powder compact in the ranges I and II, leading to a continuous densification in the rages I and II. In the ranges III and IV, the densification rate was enhanced by the addition of powder B of 60 vol.%, because the coordination number of ceria grains to a pore decreased with addition of 37 nm-powder.

Keywords: A. Sintering; B. Grain size; D. Ceria; Specific surface area

1. Introduction

Recently, sintering of nanometer-sized oxide powders has been studied for zirconia [1,2], titania [3,4], and ceria [5–7]. The decrease of a starting particle size enables the densification at a lower heating temperature because of the increased driving force (specific surface area) of sintering. On the other hand, a small pore size between ultrafine particles produces a high capillary force expressed by Eq. (1) during drying,

$$\Delta P = \frac{2\gamma \cos\theta}{r} \quad (1)$$

where ΔP is the capillary force, γ the surface tension of liquid media, θ the contact angle and r the radius of pore formed between particles. A particle size distribution of a given powder provides the related pore size distribution [8,9]. The distribution of the high ΔP values in the pores of powder compact is the origin of cracks formed during drying [10–13]. A crack-free powder compact can be prepared by decreasing γ value and increasing r value. The addition of organic liquid such as ethanol, propanol, or ethyleneglycol with a low γ value to an aqueous suspension of nanometer-sized powder was effective to prevent the formation of cracks during drying of powder compact [12,13]. In this study, the prevention of cracks in a wet compact of nanometer-sized powder was studied in relation to the mixing effect of two different-sized powders [14,15], which may be effective to reduce ΔP value by increasing r value. Ceria powders of 14 and 37 nm diameters of equivalent spherical particles were mixed in an aqueous solution at pH 6 and consolidated by filtration through a gypsum mold. The crack-free powder compacts were sintered at 500–1600 °C in air. The sinterability of the powder compacts were analyzed based on the specific surface area and the ratio of pore size to grain size of sintered compacts.

2. Experimental

A commercial 15 mass% ceria aqueous suspension (Daichi Kigenso Kagaku Kogyo, Ltd., Osaka, Japan) was

* Corresponding author. Tel.: +81 99 2858325; fax: +81 99 2574742.
E-mail address: hirata@apc.kagoshima-u.ac.jp (Y. Hirta).

0272-8842/$30.00
doi:10.1016/j.ceramint.2004.10.017

freeze-dried and calcined for 60 min at 500 °C. The calcined powder gave a specific surface area of 60.8 m^2/g (equivalent diameter of 13.9 nm, powder A). The surface state of powder A before and after the calcination was evaluated by thermogravimetric analysis (TG, Thermo plus TG 8120, Rigaku Denki Co., Tokyo, Japan) and infrared spectroscopy (IR, A-III-type, JASCO Co., Tokyo, Japan). Another commercial ceria powder with a specific surface area of 22.9 m^2/g (equivalent diameter of 36.7 nm, powder B, Daichi Kigenso Kagaku Kogyo, Ltd., Osaka, Japan) was mixed with powder A in an aqueous solution at pH 6. The shape and size of both the powders were observed by transmission electron microscope (Hitachi H-700H, Hitachi Co., Tokyo, Japan). The zeta potentials of powders A and B were measured as a function of pH at a constant ionic strength of 0.01 M NH_4NO_3 (Rank Mark II, Rank Brothers Ltd., UK).

Aqueous suspensions of 25 vol.% ceria (powder A:powder B = 90:10, 80:20, 60:40, and 40:60) at pH 6 were consolidated by filtration through a gypsum mold. Some dried powder compacts were furthermore densified by cold isostatic pressing (CIP) at 196 MPa. The ceria green compacts were heated to 500–1600 °C at a rate of 10 °C min^{-1} and sintered for 1 h. The bulk density and apparent density of sintered ceria were measured by the Archimedes method in distilled water. The porosities of closed pores (C) and open pores (O) were calculated from the apparent density ($d_1 = W/(V + C)$, where W is the mass of powder compact; V, volume fraction of solid) and bulk density ($d_2 = W/(V + O + C)$). The microstructures of sintered ceria compact were observed by scanning electron microscope (SM-300, Topcon Technologies, Inc., Tokyo, Japan). The grain size of ceria in a sintered compact was measured by line intercept method on the polished and thermally etched surface of the ceria compact. A specific surface area of sintered ceria was measured by the Brunauer–Emmett–Teller (BET) method using N_2 gas (Flowsorb 2300, Shimadzu Co., Kyoto, Japan). Table 1 summarizes the composition, processing, relative density and specific surface area of the heated ceria compacts.

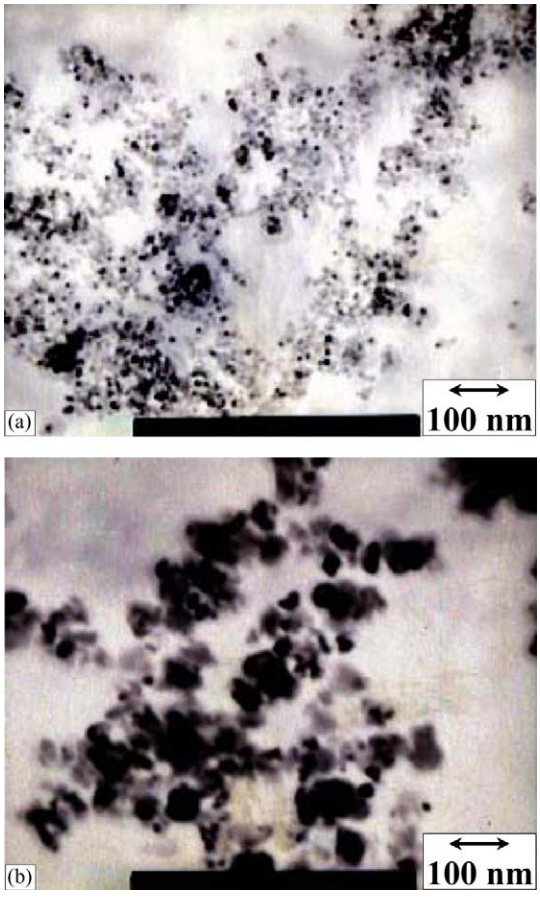

Fig. 1. Transmission electron micrographs of: (a) ceria powder A (14 nm diameter) and (b) ceria powder B (37 nm diameter).

3. Results and discussion

3.1. Characteristics and wet forming of ceria powder

Fig. 1 shows the TEM photographs of (a) powder A calcined at 500 °C and (b) as-received powder B. They consisted of equiaxed particles and the observed particle sizes were close to the diameters calculated from their specific surface areas. In the IR spectrum of freeze-dried

Table 1
Composition, processing, relative density and specific surface area of the heated ceria compacts

Sample no.	Mixing ratio (vol.%)		Consolidation[a]	Relative density (%) after heating at 500 °C	Specific surface area (m^2/g) after heating at (°C)			
	Powder A[b]	Powder B[c]			500	800	1000	1300
1	90	10	F	46.3 ± 1.2	37.1	2.3	1.5	0.62
2	90	10	F + CIP	59.6 ± 0.3	39.6	1.7	1.7	0.37
3	80	20	F	43.8 ± 0.1	31.9	3.5	1.6	0.45
4	60	40	F	50.7 ± 2.2	30.6	6.5	3.0	0.50
5	40	60	F	51.2 ± 0.3	26.0	10.0	4.0	0.79
6	40	60	F + CIP	58.0 ± 1.0	28.0	9.8	3.8	0.28

[a] F: filtration through a gypsum mold; CIP: cold isostatic pressing (196 MPa).
[b] Specific surface area 60.8 m^2/g.
[c] Specific surface area 22.9 m^2/g.

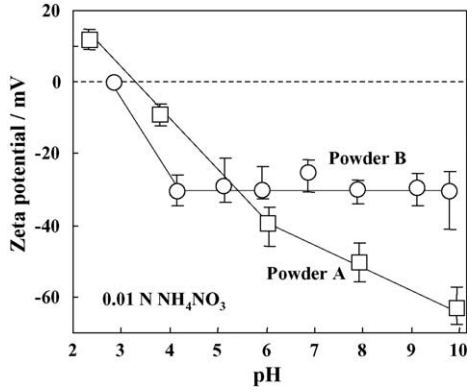

Fig. 2. Zeta potentials of ceria powders A and B as a function of suspension pH.

powder A, the adsorption bands assigned to NO_3^- groups were measured at 1620 and 1390 cm^{-1} of wave number, because the commercial powder A was supplied as a form of suspension containing HNO_3. Similarly, the adsorption bands of OH groups were detected at 1050 and 3500–3600 cm^{-1} of wave number. After the calcination of powder A at 500 °C, those bands disappeared. Fig. 2 shows the zeta potentials of powder A calcined at 500 °C and as-received powder B. Powder A was charged positively at 12 mV at pH 2.3, and was charged negatively at −8 mV at pH 3.8. The isoelectric point was pH 3.4. On the other hand, the isoelectric point of powder B was pH 3.0 and the powder was charged at −30 mV in the pH range from 4.2 to 9.8. Both the powders A and B were mixed at pH 6 for 6 h to make a 25 vol.% solid suspension. The ceria suspension was consolidated by filtration through a gypsum mold. Fig. 3 shows the appearance of the consolidated powder cakes. During the drying at room temperature, many cracks were formed on the surface of the cake from powder A suspension. The addition of 10 vol.% powder B to powder A was effective to suppress the formation of the cracks as seen in Fig. 3b. That is, the mixing of slightly large ceria particles relaxed the capillary force distributed in a wet powder compact.

3.2. Sintering behavior of ceria powders

3.2.1. Sintering temperature and relative density

Fig. 4 shows the sintering behavior of the ceria compacts with 10–60 vol.% powder B. The relative density of the powder compacts, which were consolidated by filtration and heated at 500 °C, were 43–51% (Table 1) and increased as the fraction of powder B increased. In submicrometer-sized bimodal particle systems, it is reported that the packing

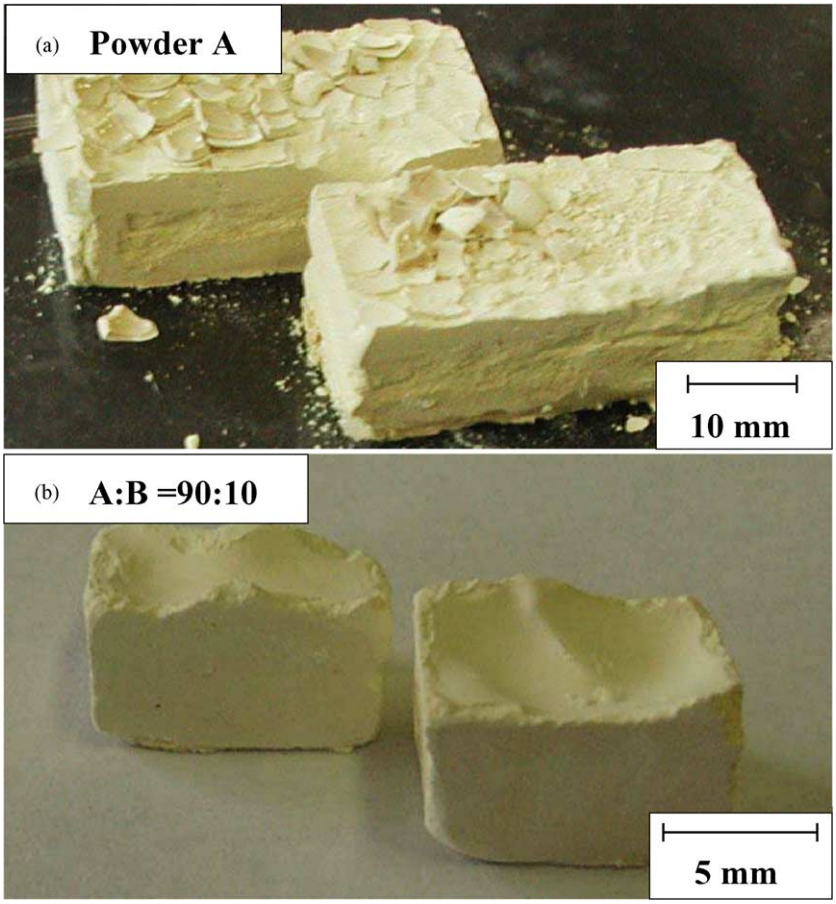

Fig. 3. Appearance of powder compacts formed by filtration of ceria suspensions of: (a) powder A and (b) 90 vol.% powder A–10 vol.% powder B.

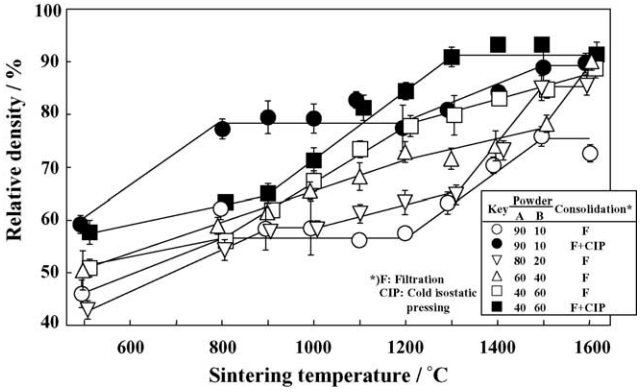

Fig. 4. Relative density of ceria compacts with 10–60 vol.% powder B after the sintering at 500–1600 °C.

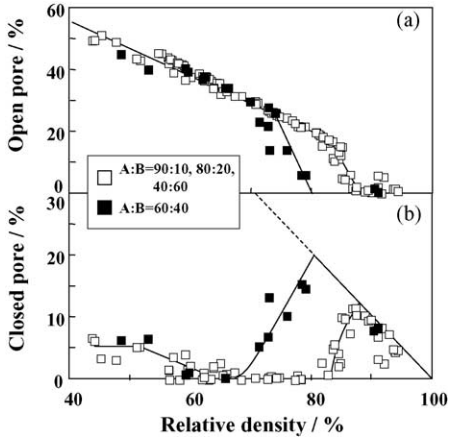

Fig. 5. Porosity of: (a) open pores and (b) closed pores in sintered ceria compacts as a function of relative density.

density of the mixed powder system becomes a maximum at the volume fraction of fine powder/coarse powder = 30/70 [15–17]. A similar increased packing density was also measured at a higher fraction of larger powder B in the present study. The cold isostatic pressing of the consolidated powder compacts with 10 and 60 vol.% powder B increased the relative density to 58–59%. The as-formed compact and subsequently CIPed compact showed a similar densification tendency with sintering temperature for the same mixing ratio of powder B (samples 1 and 2, and samples 5 and 6 in Table 1). The sintering behavior of the powder compact with 10 vol.% powder B was characterized by the following four ranges: (I) first densification range at 500–800 °C, (II) first plateau of relative density at 800–1200 °C, (III) second densification range at 1200–1500 °C and (IV) second plateau of relative density at 1500–1600 °C. When the fraction of powder B was increased above 20 vol.%, the gradual continuous densification proceeded in the ranges II (800–1200 °C) and III (1200–1500 °C). The above densification behavior is analyzed latterly.

Fig. 5 shows the porosity of open pores and closed pores in the ceria compacts as a function of relative density. The open pores disappeared at 80 and 87% relative density for the compact with 40 vol.% powder B and for the other compositions as presented in Fig. 5, respectively. The disappearance of open pores was accompanied by the formation of closed pores. The formation tendency of closed pores in sample 4 (40 vol.% powder B) is not understood at this moment. The formation of closed pores was also measured in the relative density range from 43 to 60%. That is, the densification of ceria compacts of nanometer-sized powders proceeds through the formation and disappearance of two kinds of closed pores. The closed pores at a lower relative density were formed by the sintering of primary nanometer-sized ceria particles within a secondary particle cluster (Fig. 6) [8,9]. The closed pores at a higher relative density correspond to ones formed between dense secondary particle clusters (Fig. 6). The hierarchical particle structures are closely related to the densification behavior as shown in Fig. 5.

Fig. 6 shows the schematic illustration of densification process with sintering temperature for samples 1 and 2 (10 vol.% powder B). In the range I, sintering of the nanometer-sized primary particles proceeds within secondary particle clusters. The cluster size measured in an aqueous suspension of powder B (1.75×10^{-3} vol.%) at pH 6.0 by

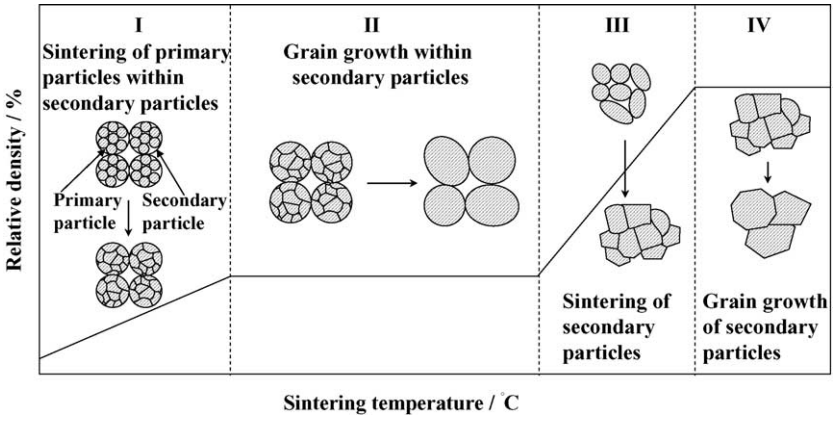

Fig. 6. Schematic illustration of sintering behavior for the nanometer-sized ceria powder compact with 10 vol.% powder B.

particle size analyzer, was 0.56 μm. The densification in the range I is characterized by the formation of closed pores at a lower relative density, measured in Fig. 5. In the range I, dense secondary particles clusters are formed. In the range II, little densification was measured for the powder compact. This result is due to the large coordination number of primary ceria grains to a pore formed between the dense secondary particle clusters. When the coordination number of grains decreases to a critical value, the densification occurs [18]. Grain growth of the primary grains within a secondary particle cluster is effective to reduce the coordination number of grains surrounding a pore. Therefore, the above grain growth proceeds in the range II, which provides the driving force for the densification during the sintering. In the range III, pores are eliminated by the sintering of dense secondary grains after the grain growth of primary grains. The densification in the range III is seen in the formation of closed pores at a higher relative density in Fig. 5. In the range IV, grain growth of dense secondary particles drastically proceeds.

3.2.2. Early stage of sintering

Fig. 7 shows the specific surface areas of ceria compacts as a function of sintering temperature. The specific surface areas of ceria compacts sintered with 10–60 vol.% powder B at 500 °C were 26–40 m^2/g (Table 1). After the sintering at 800 °C, the specific surface areas decreased to 1.7–10 m^2/g in the ceria compacts with 10–60 vol.% powder B. The consolidation methods (filtration, cold isostatic pressing) gave no influence on the specific surface area of the ceria compacts of numbers 1 and 2 (10 vol.% powder B) and numbers 5 and 6 (60 vol.% powder B). The large decrease in

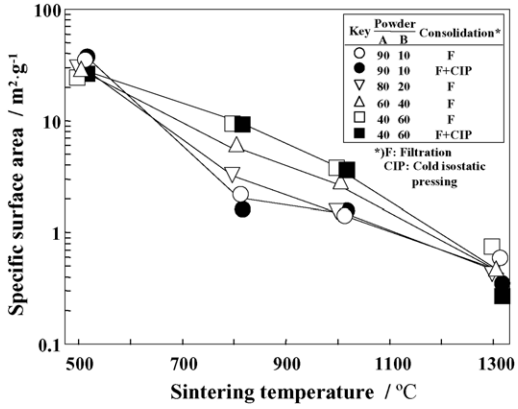

Fig. 7. Specific surface areas for the ceria compacts with 10–60 vol.% powder B after the sintering at 500–1300 °C.

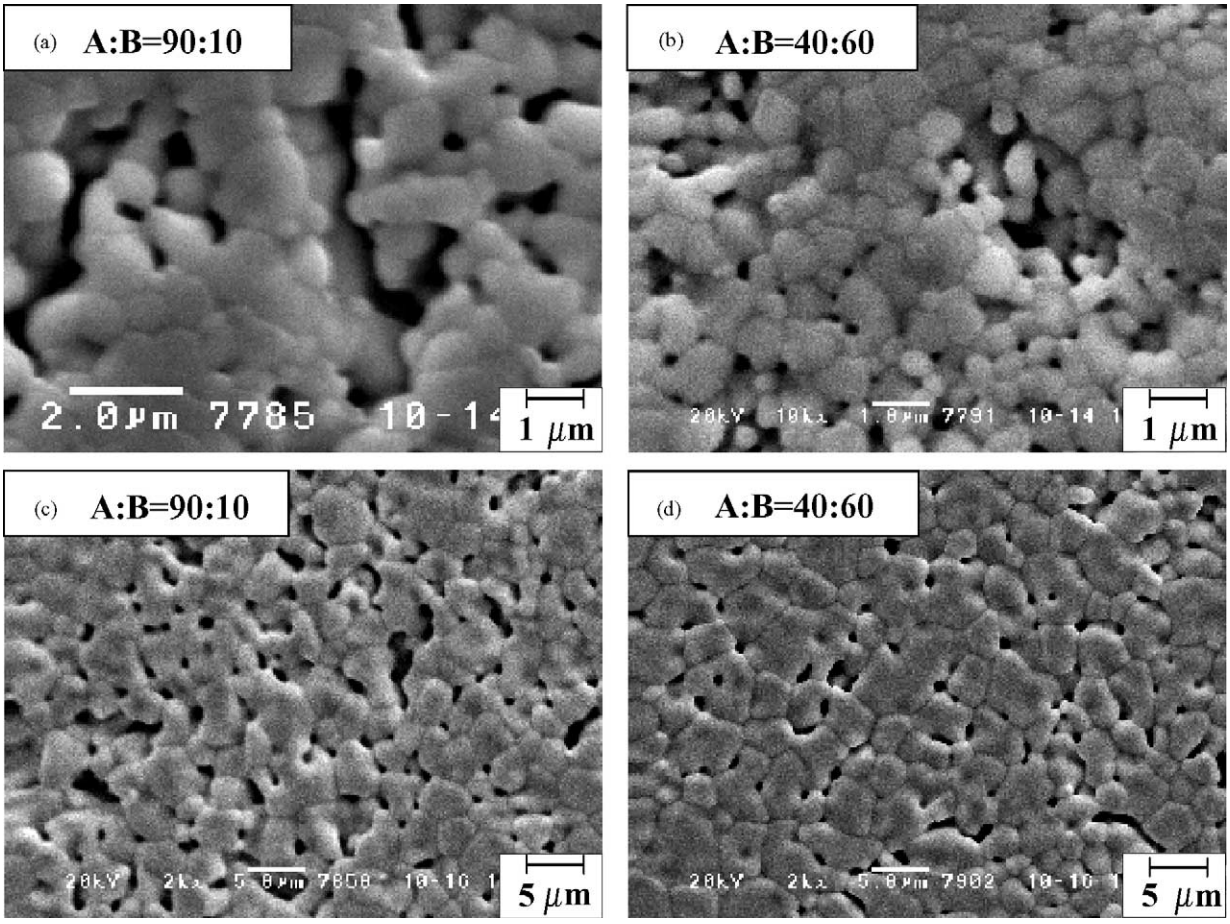

Fig. 8. Microstructures of ceria sintered at 1300 °C (a and b) and 1500 °C (c and d).

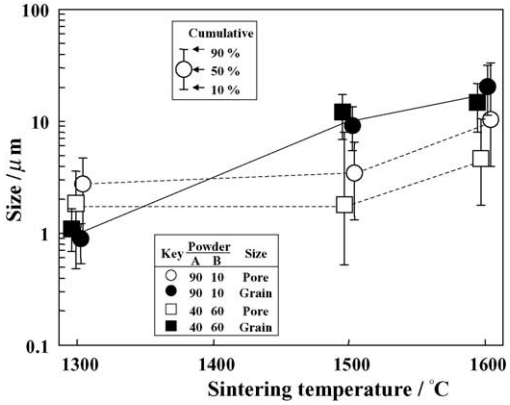

Fig. 9. Distributions of pore size and grain size of ceria compacts, which were consolidated by filtration plus cold isostatic pressing and sintered at 1300–1600 °C.

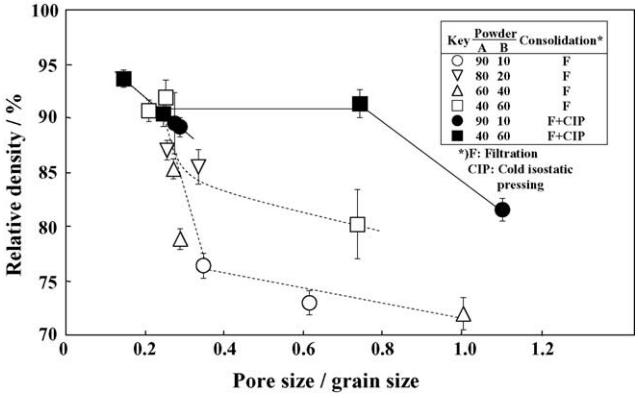

Fig. 10. Relationship between relative density and ratio of pore size to grain size for the ceria compacts sintered at 1300–1600 °C.

the specific surface area for the ceria compact with 10 vol.% powder B in the range I, is related to the enhanced densification by the sintering (Fig. 4). The green density plays a key role for the bulk density after the sintering. In the range II, small decrease of the specific surface area was measured for the ceria compact with 10 vol.% powder B, supporting the grain growth process within dense particle clusters shown in Fig. 6. On the other hand, the ceria compacts with 40–60 vol.% powder B (samples 4–6) showed a gradual decrease of the specific surface area in the ranges I and II. This result corresponds to the gradual increase of the relative density in the ranges I and II. The above results indicate that the addition of large nanometer-sized ceria powder (>40 vol.% powder B) to powder A suppresses the decrease of the specific surface area of the powder compact at a higher sintering temperature. As a result, the densification behavior of the powder compact is greatly affected by the composition of mixed powders.

3.2.3. *Intermediate to final stages of sintering*

The densification process at a temperature higher than 1300 °C was independent of the specific surface area of the powder compact. The specific surface areas for all the ceria compacts with 10–60 vol.% decreased to the values lower than 1 m^2/g after the sintering at 1300 °C (Fig. 7). Another driving force for the densification is proposed in the range III in Fig. 6. Fig. 8 shows the microstructures of ceria compacts sintered with 10 and 60 vol.% powder B at 1300 °C (a and b) and 1500 °C (c and d). The increase of the sintering temperature promoted the densification with grain growth for both the compacts. The grain growth reduces the coordination number of grains surrounding a large pore as seen in Fig. 8. The quantitative values of grain size and pore size are shown in Fig. 9 for the ceria compacts with 10 and 60 vol.% powder B, formed by filtration plus cold isostatic pressing. The pore size was almost constant in the range III (1300–1500 °C) and increased in the range IV (1500–1600 °C) for both the compositions. The increased fraction of powder B (60 vol.%) produced smaller pores. On the other hand, the grain size of ceria increased continuously in the ranges III and IV. The mixing ratio of powder A to powder B gave no significant influence on the grain size of ceria. These changes in the grain size and pore size effectively reduced the ratio of pore size to grain size with increasing temperature. That is, the coordination number of ceria grains to a pore decreased at a higher sintering temperature in the range III.

Fig. 10 summarizes the relationship between the ratio of pore size to grain size and relative density of powder compacts with 10–60 vol.% powder B in the ranges III and IV. It is apparent that the densification is enhanced as the ratio of pore size to grain size decreased. The decrease of coordination number of grain to a pore is a driving force of sintering in the ranges III and IV. The difference in the relative density with powder composition or consolidation process in Fig. 10 reflects the microstructure and bulk density of green compacts as seen in Figs. 4 and 9. A similar result is also reported by Chen and Chen [19].

4. Conclusions

(1) Formation of cracks in the ceria compact produced from an aqueous suspension of 14 nm-powder during drying in air, was suppressed by mixing of 37 nm-ceria powder at 10 vol.%.
(2) Densification process of the ceria powder compact with 10 vol.% of 37 nm-powder was divided into four ranges with sintering temperature: range I (500–800 °C)—sintering of nanometer-sized primary particles within a secondary particle cluster, range II (800–1200 °C)—grain growth of primary particles in a dense secondary particle cluster, range III (1200–1500 °C)—sintering of dense secondary particle clusters with grain growth, and range IV (1500–1600 °C)—grain growth of dense secondary particle clusters.
(3) In the range II, the addition of 37 nm-powder in the fractions above 40 vol% to 14 nm-powder enhanced the

densification because of the gradual decrease of the specific surface area with increasing sintering temperature.

(4) The addition of 37 nm-powder (60 vol.%) to 14 nm-powder (40 vol.%) suppressed the growth of pores in the range III but gave a small influence on the grain growth of ceria. As a result. the densification rate of the ceria compact was enhanced by the addition of 37 nm-powder to 14 nm-powder because of the decrease of the coordination number of ceria grains.

References

[1] V.V. Srdic, M. Winterer, H. Hahn, Sintering behavior of nanocrystalline zirconia prepared by chemical vapor synthesis, J. Am. Ceram. Soc. 83 (4) (2000) 729–736.

[2] G. Skandan, H. Hahn, M. Roddy, W.R. Cannon, Ultrafine-grained dense monoclinic and tetragonal zirconia, J. Am. Ceram. Soc. 77 (7) (1994) 1706–1710.

[3] R.W. Siegel, S. Ramasamy, H. Hahn, L. Zongquan, L.U. Ting, R. Gronsky, Synthesis, characterization and properties of nanophase TiO_2, J. Mater. Res. 3 (6) (1988) 1367–1372.

[4] H. Hahn, J. Logas, R.S. Averback, Sintering characteristics of nanocrystalline TiO_2, J. Mater. Res. 5 (3) (1990) 609–614.

[5] Y. Zhou, R.J. Philips, J.A. Switzer, Electrochemical synthesis and sintering of nanocrystalline cerium (IV) oxide powders, J. Am. Ceram Soc. 78 (4) (1995) 981–985.

[6] P.L. Chen, I.W. Chen, Sintering of fine oxide powders: II. Sintering mechanism, J. Am. Ceram. Soc. 80 (3) (1997) 637–645.

[7] P. Duran, F. Capel, D. Gutierrez, J. Tartaj, C. Moure, Cerium (IV) oxide synthesis and sinterable powders prepared by the polymetric organic complex solution method, J. Eur. Ceram. Soc. 22 (2002) 1711–1721.

[8] Y. Hirata, I.A. Aksay, R. Kikuchi, Quantitative analysis of hierarchical pores in powder compact, J. Ceram. Soc. Jpn. 98 (2) (1990) 126–135.

[9] Y. Hirata, Theoretical aspects of colloidal processing, Ceram. Int. 23 (1997) 93–98.

[10] G.W. Scherer, Theory of drying, J. Am. Ceram. Soc. 73 (1) (1990) 3–14.

[11] R.G. Horn, Surface forces and their action in ceramic materials, J. Am. Ceram. Soc. 73 (5) (1990) 1117–1135.

[12] Y. Hirata, K. Takeshima, Y. Ishihara, Synthesis of whisker reinforced mullite matrix composites using colloidal processing, J. Ceram. Soc. Jpn. 100 (4) (1992) 353–361.

[13] K. Koushio, S. Uchida, S. Sameshima, Y. Hirata, Formation of solid electrolyte films by transfer printing method, in: Proceedings of the 19th Korea–Japan International Seminar on Ceramics, 2002587–591.

[14] Y. Hirata, S. Matsushita, S. Nakagama, Y. Ishihara, S. Hori, Rheological properties and consolidation of the suspension in the alumina powder–silicon nitride whisker system, J. Ceram. Soc. Jpn. 97 (9) (1989) 881–887.

[15] Y. Hirata, S. Nakagama, Y. Ishihara, Forming of the alumina powder–silicon nitride whisker system with aqueous suspension, Trans. Mater. Res. Soc. Jpn. 5 (1992) 47–67.

[16] J.L. Shi, J.D. Zhang, Compaction and sintering behavior of bimodal alumina powder suspension by pressure filtration, J. Am. Ceram. Soc. 83 (4) (2000) 737–742.

[17] B.V. Velamakanni, F.F. Lange, Effect of interparticle potentials and sedimentation on particle packing density of bimodal particle distribution during pressure filtration, J. Am. Ceram. Soc. 74 (1) (1991) 166–172.

[18] W.D. Kingary, H.K. Bowen, D.R. Uhlmann, Introduction to Ceramics, John Wiley & Sons Inc, New York, 1976, pp. 469–490.

[19] P.L. Chen, I.W. Chen, Sintering of fine oxide powders: I. Microstructural evolution, J. Am. Ceram. Soc. 79 (12) (1996) 3129–3141.